Additive Manufacturing feasibility of WC-17Co cermet parts by Laser Powder Bed Fusion

Kevin Papy, Jean-Marc Staerck, Alexey Sova, András Borbély

Available online at www.sciencedirect.com

ScienceDirect

Procedia CIRP 111 (2022) 153–157

www.elsevier.com/locate/procedia

12th CIRP Conference on Photonic Technologies [LANE 2022], 4-8 September 2022, Fürth, Germany

Additive Manufacturing feasibility of WC-17Co cermet parts by Laser Powder Bed Fusion

Kevin Papy[a]*, Staerk Jean-Marc[a], Sova Alexey[b], Borbely Andras[c]

[a] *Technogenia, Saint-Jorioz, France.*
[b] *University of Lyon, Ecole Centrale de Lyon - ENISE, LTDS, UMR CNRS 5513, Saint Etienne, France,*
[c] *Mines Saint-Etienne, Univ Lyon, CNRS, UMR 5307 LGF, Centre SMS, F - 42023 Saint-Etienne France*

* Corresponding author. Tel.: +3 06 82 23 01 80; *E-mail address:* kevin.papy@technogenia.com

Abstract

Cermets are composite materials consisting of a ceramic reinforcement and a metal matrix. Laser Powder Bed Fusion (L-PBF) is an Additive Manufacturing (AM) technology. The present paper deals with the feasibility study of AM of cermet parts by L-PBF using WC-17Co powder. The results showed that parametric optimization of the L-PBF process allowed the production of solid WC-17Co part. Structural analysis revealed the presence of significant porosity (1.41%) and small-scale cracks in the as-built samples. Post-processing by HIP (Hot Isostatic Pressure) significantly improved the structure of manufactured parts. The porosity became very low (0.01%) and XRD phase analysis revealed the absence of the fragile W_2C phase. Abrasive wear and hardness tests showed that performances of additively manufactured parts were comparable to a reference part produced by powder sintering. The study successfully demonstrated the possibility of manufacturing wear-resistant cermet parts

Peer-review under responsibility of the international review committee of the12th CIRP Conference on Photonic Technologies [LANE 2022]

Keywords: Cermet; Tungsten Carbide; Additive Manufacturing; Laser Powder Bed Fusion; Hot Isostatic Pressing

1. Introduction

Laser power bed fusion (L-PBF), also known as selective laser melting (SLM), is an additive manufacturing process employed for the production of complex functional parts using metal powder as feedstock material. In L-PBF, a laser beam is applied to melt the powder material and form three-dimensional parts employing the layer-by-layer approach. The final properties of the built parts, such as roughness, density, porosity, cracking propensity, and mechanical properties, depend on process parameters, such as laser power, scanning speed, and layer thickness [1]–[6]. Considering several studies, it can be concluded that L-PBF manufacturing of WC-Co parts remains challenging [7]–[11]. Preheating of the building plate to a high temperature allowed the manufacturing of solid samples with some residual porosity that could be eliminated through post-treatment [12]–[14]. However, in the absence of a preheating plate option, the manufacturing of complex-shaped WC-Co parts, even with high internal porosity, was not possible owing to crack formation and the destruction of the part during cutting from the plate [15], [16]. Considering the available literature data, this study will focus on the following:

- Optimization of the L-PBF parameters for the manufacture of solid complex-shaped WC-17Co parts without the use of a preheated plate.
- Analysis of the effect of hot isostatic pressing (HIP) on the structure and properties of WC-17Co produced using L-PBF.

2212-8271
Peer-review under responsibility of the international review committee of the12th CIRP Conference on Photonic Technologies [LANE 2022]
10.1016/j.procir.2022.08.049

Nomenclature

AM	Additive Manufacturing
L-PBF	Laser Powder Bed Fusion
SLM	Selective Laser Melting
ICP-MS	Inductively Coupled Plasma Mass Spectrometry
XRD	X-Ray Diffraction
EBSD	Electron Back Scattered Diffraction
HIP	Hot Isostatic Pressure
E_V	Volume Energy Density
P	Power
V_s	Scan Speed
H_d	Hatching Distance
l	Layer thickness

2. Material and methods

2.1. L-PBF Equipment

Pro X 200 DMP equipment supplied by 3D Systems was used in the study. The volume of the working chamber where the parts were manufactured was 140 × 140 × 125 mm^3. The L-PBF machine was equipped with a 400 W fiber laser with a wavelength of 1070 nm. The working chamber was filled with nitrogen during manufacturing to prevent oxidation. It is important to note that the analysis of the laser beam quality revealed a significant effect of the laser power on the energy distribution in the beam. In particular, for powers higher than 200 W and long exposure times, the energy distribution changed from a Gaussian spot to a ring shape. Evidently, this effect introduces an additional process parameter that significantly complicates the optimization process. To avoid the influence of energy distribution on the optimized parameters, the maximum laser power applied in the experiments was set to 160 W, when the shape of the energy distribution surface remained close to Gaussian. The spot diameter was 130 µm. The laser power and scan velocity were varied from 100 to 160 W and from 30 to 200 mm/s, respectively. Layer thickness of 30 µm was applied. No build plate preheater was used during the study.

2.2. Powder

Agglomerated-sintered WC-17Co powder with a particle size distribution of 15–53 µm (Oerlikon Metco) was used in this study. The powder was initially developed for thermal spray applications, such as HVOF and HVAF. SEM images of the particles and their cross-sections are presented in Figure 1. From the SEM images, it is evident that the particles are quasi-spherical in shape. The cross-sectional images revealed the presence of internal porosity. The average size of the WC grains (dark grey phase) was estimated to be 4-5 µm. The carbide grains were uniformly distributed in the cobalt matrix (light grey phase).

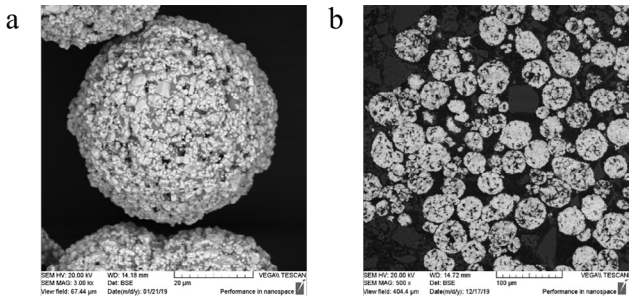

Fig. 1. SEM images of (a) the WC-17Co particles and (b) their cross-sections

The inductively coupled plasma mass spectrometry (ICP-MS) analysis results are presented in Table 1. The chemical composition determined using ICP-MS was within the range stated by the supplier. However, it did not correspond exactly to the result declared by the powder supplier. XRD measurement conducted on initial powder shown only WC (P-6m2) and Co (Fm-3m) phases.

Table 1. Chemical analysis of the initial powder employing ICP-MS.

Element [wt.%]		
W	C	Co
76.4	5.2	18.4

2.3. Post-treatment processes

Cube-shaped samples with dimensions of 10 × 10 × 10 mm^3 manufactured using L-PBF were used for post-treatment. A batch was subjected to capsule-free HIP, which is a cycle applied during industrial processes. The HIP process was performed in several steps. First, the temperature was gradually increased from room temperature to 1000 °C over 15 h under normal pressure. The temperature was then increased to the sintering temperature of 1450 °C at a heating rate of 5 °C/min in a pressure furnace maintained at 40 MPa, and these conditions were held for 5 h. Cooling to room temperature was performed in the HIP chamber at a rate of 6 °C/min.

2.4. Structural and mechanical properties

The relative density of the manufactured parts was determined by the Archimedes method according ASTM-B962. Image analysis was performed using ImageJ [17]. The microstructure and element distribution were analyzed using a Zeiss Supra 55VP v2 scanning electron microscope (SEM). Vickers hardness (HV) was determined by applying a load of 30 kg for 10 s to all samples [18]. The wear resistance of the materials was measured following the ASTM G-65 standard [19] using dry sand and a rubber wheel. Samples with dimensions of 25 × 60 × 7 mm^3 were used for the wear resistance tests. The abrasion wear test conditions are listed in Table 2.

Table 2 : Abrasion wear test conditions.

Abrasive	Abrasive flow, [g/min]	Wheel revolution [nb]	Abrasion length, [m]	Applied load, [N]	Test duration, [min]
Silica sand (125-400)	300	6000	4309	130	30

3. Results and discussion

3.1. Optimization of process parameters

In the first step, the parametric window of the L-PBF process was determined. The principal purpose of these experiments was to determine the parameters that enable the production of materials with the lowest porosity and least cracks. Initially, single tracks were deposited with a powder layer thickness of 30 µm. The power and scan velocity were varied from 100 to 160 W and from 30 to 200 mm/s, respectively. Table 3 summarizes the parameter ranges tested in the first stage.

Table 3 : Ranges of L-PBF manufacturing parameters applied in the experiments

Layer thickness [µm]	30
Range of laser power [W]	100-130-160
Range of scan speed [mm/s]	30-100
Range of hatching distance [µm]	140-200
Inert gas	Nitrogen

Analysis of the track shape revealed that stable tracks were formed only when the scanning speed was in the 30-40 mm/s range at a laser power of 130 W. Following the single-track experiments, 3D objects with simple geometries (cubes and parallelepipeds) were manufactured. Numerous factors can affect the process results, such as the laser power, scan speed, hatch spacing, layer thickness, and scanning strategy. These factors are important because re-melting depends on the amount of volumetric energy density (E_v) absorbed during the process as defined by the following equation:

$$E_v = \frac{P}{Vs \times Hd \times l} \quad (1)$$

where E_v is the energy density (J/mm^3), P is the laser power (W), Vs is the scanning speed (mm/s), Hd is the hatch distance (mm), and l is the layer thickness (mm). Similar approaches based on energy density optimization in the L-PBF process have already been successfully applied several times [20]–[22]. Furthermore, hexagonal and zigzag scanning strategies were applied to produce WC-Co cubes (Figure 2).

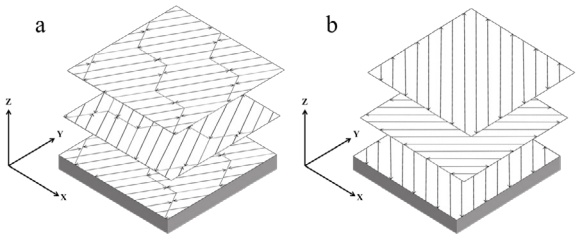

Fig. 2. Schematic illustration of (a) zigzag and (b) hexagonal scanning strategies

To analyze the porosity and other defects, the samples were cut in XZ plane. Figure 3 shows the relationship between sample porosity and energy density.

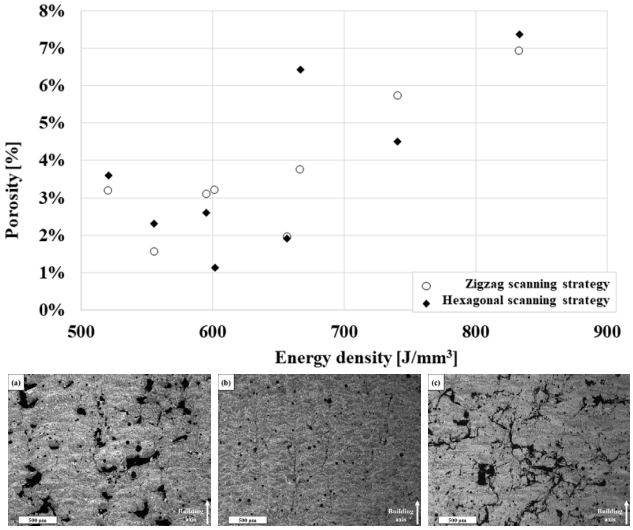

Fig. 3. Top: plot of sample porosity vs. energy density for zigzag and hexagonal scanning strategies. Bottom: SEM images of samples manufactured via the hexagonal scanning strategy at (a) (520 J/mm^3), (b) 602 J/mm^3, and (c) 833 J/mm^3

The plot in Figure 3 indicates that samples with the highest density (98.6%) were manufactured using an energy input of 602 J/mm^3 and the hexagonal scanning strategy (Figure 4b). The samples manufactured at a lower energy density (hexagonal scanning strategy) were significantly more porous, and the pore size was significantly larger (Figure 4a). This dramatic increase in porosity could be explained by the lack of fusion of the WC-Co powder. An increase in the energy density to > 602 J/ mm^3 led to crack formation at the layer interface. The samples manufactured at 833 J/mm^3 using the hexagonal scanning strategy contained abundant cracks and had the lowest density, which indicates a high level of residual stress. For the samples produced employing the zigzag scanning strategy, the optimum energy density was found to be 560 J/mm^3. However, in general, the densities of the zig-zag-generated samples were lower than those produced using the hexagonal scanning strategy. Thus, the final batch of samples was produced using the hexagonal strategy. HIP treatment was used to close the cracks and the pores.

3.2. Microstructure and composition of different samples

SEM images of the sample produced at 602 J/mm^3 applying the hexagonal manufacturing strategy and the sample after HIP treatment are shown in Figure 4. Microstructure observations revealed that unlike the powder, the as-built samples contained significantly finer carbide grains. In particular, plenty of grains with a size of ~1-3 µm were visible, but some submicron carbide inclusions were also present in the metal matrix. Cracks and pores were visible throughout the sample. However, these defects did not affect the integrity of the cube. HIP of the as-built samples significantly modified their microstructures and crystallographic phases. In particular, cracks were no longer visible in the cross-section images (Figure 4b), because high temperature and the external pressure promote material diffusion, allowing for crack closure and sintering of the contact surfaces.

According to image analysis results, the relative density of the as-built samples was 98.59%, in contrast, the effect of HIP on porosity was remarkable with a relative density of approximately 99.99%.

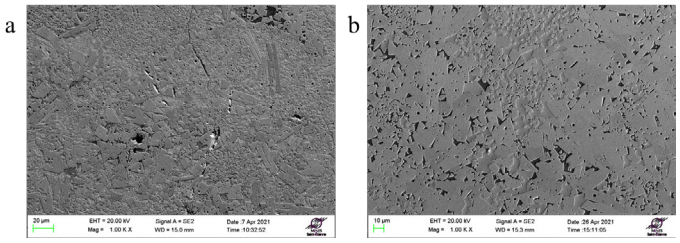

Fig. 4. Sample microstructures of (a) as-built and (b) HIP

X-ray diffraction was employed for phase analysis using an X'PertPro MPD diffractometer with CuKα radiation, Rietveld refinement was perfomred using the MAUD software [23]. A Ni filter was set in the beam to remove the CuKβ spectral component.

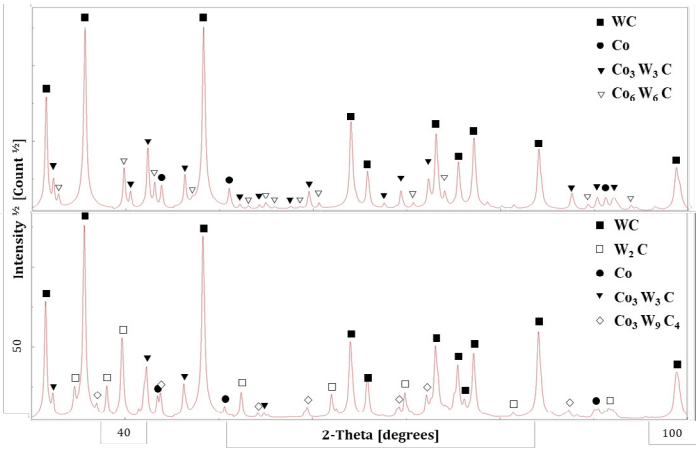

Fig. 5. XRD patterns of the (Bottom) as-built and (Top) HIP-treated samples.

The results of the XRD analysis performed on the as-built and HIP samples are shown in Figure 5. Complex carbide phases formed during the L-PBF process were detected in the XRD patterns of the as-built samples. In particular, the W_2C, ternary Co_3W_3 C, and Co_3W_9 C_4 phases were present in the as-built samples. These phases present compact hexagonal (P63/mmc), cubic (Fd-3m), and compact hexagonal structures (P63/mmc), respectively. The XRD patterns of the HIP samples are presented at the top of Figure 5. The phase transformation induced during HIP at high temperature resulted in the complete dissolution of the fragile W_2C phase. Meanwhile, formation of the Co_6W_6C phase with a cubic structure (Fd-3m) was observed. It can be concluded that the temperature of 1450 °C during treatments was the key factor influencing the final phase composition.

3.3 Macrohardness and wear resistance

Macrohardness tests were performed on the as-built and HIP-treated samples. Three measurements were performed per sample according to the standard methods, the results are shown in Table 4. The mean value obtained for the as-built samples was 1096 HV_{30}, which is close to those obtained for WC-17Co parts manufactured using powder sintering [24]–[26]. In addition, material cracking was observed near the corners of the indent , which indicated high material brittleness (Figure 6a). The hardness of the HIP-treated (1152 HV_{30}) samples was slightly higher than that of the as-built samples and material cracking occurred to a significantly lower extent, likely due to elimination of the fragile W_2C phase.

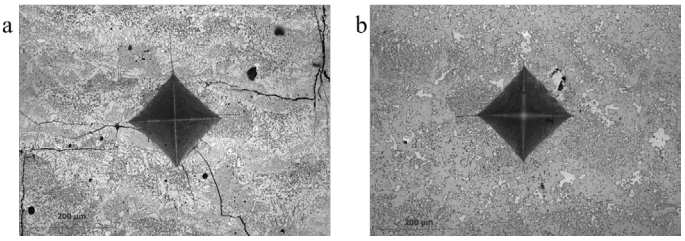

Fig. 6. Overview Vickers indent on the surface of the (a) as-built and (b) HIP samples

The results of the abrasion wear tests are summarized in Table 4. The wear rate is represented by volume loss.

Table 4: Results of the mechanical test.

Sample	Density [g/cm³]	Volume loss [mm³]	Hardness [HV_{30}]
As-built	14.30	4.20 ± 0.4	1096 ± 40
HIP	14.66	5.29 ± 0.8	1152 ± 17

The density and volume loss of the HIP treated parts was slightly higher than for the as-built parts, which can be caused by larger carbides grown during HIP. Previously reported results indicated that WC-17Co parts obtained via conventional powder sintering exhibited comparable density and volume loss during the wear resistance test in accordance with the ASTM G 65 standard [27]–[29].

Conclusion

The feasibility of L-PBF additive manufacturing without a preheated plate to generate dense cermet samples from WC-17Co was successfully assessed. The results can be summarized as follows:

- The manufacture of WC-17Co parts using L-PBF without plate preheating was found to be feasible despite the presence of porosities and cracks. Samples with the lowest porosity fraction (1.4%) and highest integrity were obtained using a volume energy density of 602 J/mm³. The as-built samples contained the brittle W_2C phase and some small-scale pores and cracks.
- The sample structure, density, and hardness can be significantly improved through capsule-free HIP, resulting in close-to-zero porosity and no cracks. HIP allowed the dissolution of the undesirable brittle W_2C phase. Other complex carbides, such as Co_3W_3C, $Co_3W_9C_4$, and Co_6W_6C, observed in the as-built samples were also present after HIP.
- The macrohardness and abrasive wear resistance of the L-PBF-manufactured WC-17Co parts were comparable to the values obtained for the sintered reference samples.

References

[1] E. Herderick, "Additive manufacturing of metals: A review," *Materials Science and Technology Conference and Exhibition 2011, MS and T'11*, vol. 2, no. 176252, pp. 1413–1425, 2011.

[2] N. Li *et al.*, "Progress in additive manufacturing on new materials: A review," *Journal of Materials Science and Technology*, vol. 35, no. 2, pp. 242–269, 2019, doi: 10.1016/j.jmst.2018.09.002.

[3] B. Zhang, Y. Li, and Q. Bai, "Defect Formation Mechanisms in Selective Laser Melting: A Review," *Chinese Journal of Mechanical Engineering (English Edition)*, vol. 30, no. 3, pp. 515–527, 2017, doi: 10.1007/s10033-017-0121-5.

[4] S. Vock, B. Klöden, A. Kirchner, T. Weißgärber, and B. Kieback, "Powders for powder bed fusion: a review," *Progress in Additive Manufacturing*, vol. 4, no. 4, pp. 383–397, 2019, doi: 10.1007/s40964-019-00078-6.

[5] Ian Gibson, Brent Stucker, and David Rosen, *Additive Manufacturing Technologies 3D Printing, Rapid Prototyping,and Direct Digital Manufacturing*, vol. Second Edition. 2019. doi: 10.1007/978-1-4939-2113-3.

[6] C. Y. Yap *et al.*, "Review of selective laser melting: Materials and applications," *Applied Physics Reviews*, vol. 2, no. 4, 2015, doi: 10.1063/1.4935926.

[7] A. Domashenkov, A. Borbély, and I. Smurov, "Structural modifications of WC/Co nanophased and conventional powders processed by selective laser melting," *Materials and Manufacturing Processes*, vol. 32, no. 1, pp. 93–100, 2017, doi: 10.1080/10426914.2016.1176195.

[8] S. Kumar and A. Czekanski, "Optimization of parameters for SLS of WC-Co," *Rapid Prototyping Journal*, vol. 23, no. 6, pp. 1202–1211, 2017, doi: 10.1108/RPJ-10-2016-0168.

[9] D. Bricin and A. Kriz, "Processability of WC-CO powder mixtures using slm additive technology," *MM Science Journal*, vol. 2019, no. June, pp. 2939–2944, 2019, doi: 10.17973/MMSJ.2019_06_2018115.

[10] M. Al-Thamir, D. G. McCartney, M. Simonelli, R. Hague, and A. Clare, "Processability of atypical WC-Co composite feedstock by laser powder-bed fusion," *Materials*, vol. 13, no. 1, pp. 1–12, 2020, doi: 10.3390/ma13010050.

[11] R. S. Khmyrov, V. A. Safronov, and A. v. Gusarov, "Synthesis of Nanostructured WC-Co Hardmetal by Selective Laser Melting," *Procedia IUTAM*, vol. 23, pp. 114–119, 2017, doi: 10.1016/j.piutam.2017.06.011.

[12] D. Bricín *et al.*, "Development of the structure of cemented carbides during their processing by slm and hip," *Metals*, vol. 10, no. 11, pp. 1–17, 2020, doi: 10.3390/met10111477.

[13] E. Uhlmann, A. Bergmann, and W. Gridin, "Investigation on Additive Manufacturing of Tungsten Carbide-cobalt by Selective Laser Melting," *Procedia CIRP*, vol. 35, pp. 8–15, 2015, doi: 10.1016/j.procir.2015.08.060.

[14] Schwanekamp, "Thermal Post-Treatment of Additively Manufactured WC-Co Processed by Laser Powder Bed Fusion," 2019.

[15] T. Schwanekamp, "Parameter study on laser beam melting of WC- Co at 800 ° C pre-heating temperature," *ICAT Proceedings of 7th International Conference on Additive Technologies*, no. October, pp. 78–84, 2019.

[16] T. Schwanekamp and M. Reuber, "Additive manufacutring of application optimized tungsten carbide precision tools," *6 th International Conference on Additive Technologies*, no. January 2016, pp. 100–114, 2016, doi: 10.1016/S0925-8388(03)00637-6.

[17] "ImageJ", [Online]. Available: https://imagej.nih.gov/ij/

[18] "Hardmetas - Palmqvist toughness test - ISO28079." 2009.

[19] ASTM International, "G65-16: Standard Test Method for Measuring Abrasion Using the Dry Sand / Rubber Wheel," *ASTM Standards*, vol. 04, no. Reapproved 2010, pp. 1–12, 2013.

[20] K. G. Prashanth, S. Scudino, T. Maity, J. Das, and J. Eckert, "Is the energy density a reliable parameter for materials synthesis by selective laser melting?," *Materials Research Letters*, vol. 5, no. 6, pp. 386–390, 2017, doi: 10.1080/21663831.2017.1299808.

[21] I. U. A.M. Mancisidor, F. Garciandia, M. San Sebastian, P.Alvarez, J.Diaz, "Reduction of residual porosity in parts manufactured by selective laser melting using skywriting and high focus offset strategies.," *Physics Procedia*, vol. 83, pp. 864–873, 2016, doi: 10.1016/j.phpro.2016.08.090.

[22] J. P. Oliveira, T. G. Santos, and R. M. Miranda, "Revisiting fundamental welding concepts to improve additive manufacturing: From theory to practice," *Progress in Materials Science*, vol. 107, no. June 2019, p. 100590, 2020, doi: 10.1016/j.pmatsci.2019.100590.

[23] "MAUD", [Online]. Available: http://maud.radiographema.eu/

[24] D. K. Shetty, I. G. Wright, P. N. Mincer, and A. H. Clauer, "Indentation fracture of WC-Co cermets," *Journal of Materials Science*, vol. 20, no. 5, pp. 1873–1882, 1985, doi: 10.1007/BF00555296.

[25] H. Materials *et al.*, "Fracture toughness of cemented carbides : Testing method and microstructural effects," *International Journal of Refractory Metals and Hard Materials*, 2014.

[26] B. Roebuck, E. Bennett, L. Lay, and R. Morrell, "Palmqvist Toughness for Hard and Brittle Materials Measurement Good Practice Guide No . 9," no. 9, p. 48, 2008.

[27] M. Antonov, R. Veinthal, D. L. Yung, D. Katušin, and I. Hussainova, "Mapping of impact-abrasive wear performance of WC-Co cemented carbides," *Wear*, vol. 332–333, pp. 971–978, 2015, doi: 10.1016/j.wear.2015.02.031.

[28] I. Konyashin and B. Ries, "Wear damage of cemented carbides with different combinations of WC mean grain size and Co content. Part I: ASTM wear tests," *International Journal of Refractory Metals and Hard Materials*, vol. 46, pp. 12–19, 2014, doi: 10.1016/j.ijrmhm.2014.04.021.

[29] A. J. Gant and M. G. Gee, "Wear of tungsten carbide-cobalt hardmetals and hot isostatically pressed high speed steels under dry abrasive conditions," *Wear*, vol. 250–251, no. PART 2, pp. 908–915, 2001, doi: 10.1016/s0043-1648(01)00749-9.